PROCEEDINGS OF SPIE

Infrared Technology and Applications XXXIV

Bjørn F. Andresen
Gabor F. Fulop
Paul R. Norton
Editors

17–20 March 2008
Orlando, Florida, USA

Sponsored and Published by
SPIE

Part One of Two Parts

Volume 6940

Proceedings of SPIE, 0277-786X, v. 6940

The papers included in this volume were part of the technical conference cited on the cover and title page. Papers were selected and subject to review by the editors and conference program committee. Some conference presentations may not be available for publication. The papers published in these proceedings reflect the work and thoughts of the authors and are published herein as submitted. The publisher is not responsible for the validity of the information or for any outcomes resulting from reliance thereon.

Please use the following format to cite material from this book:
Author(s), "Title of Paper," in *Infrared Technology and Applications XXXIV*, edited by Bjørn F. Andresen, Gabor F. Fulop, Paul R. Norton, Proceedings of SPIE Vol. 6940 (SPIE, Bellingham, WA, 2008) Article CID Number.

ISSN 0277-786X
ISBN 9780819471314

Published by
SPIE
P.O. Box 10, Bellingham, Washington 98227-0010 USA
Telephone +1 360 676 3290 (Pacific Time) · Fax +1 360 647 1445
SPIE.org

Printed in the United States of America.

Publication of record for individual papers is online in the SPIE Digital Library.

SPIE Digital Library

SPIEDigitalLibrary.org

Paper Numbering: Proceedings of SPIE follow an e-First publication model, with papers published first online and then in print and on CD-ROM. Papers are published as they are submitted and meet publication criteria. A unique, consistent, permanent citation identifier (CID) number is assigned to each article at the time of the first publication. Utilization of CIDs allows articles to be fully citable as soon they are published online, and connects the same identifier to all online, print, and electronic versions of the publication. SPIE uses a six-digit CID article numbering system in which:

- The first four digits correspond to the SPIE volume number.
- The last two digits indicate publication order within the volume using a Base 36 numbering system employing both numerals and letters. These two-number sets start with 00, 01, 02, 03, 04, 05, 06, 07, 08, 09, 0A, 0B … 0Z, followed by 10-1Z, 20-2Z, etc.

The CID number appears on each page of the manuscript. The complete citation is used on the first page, and an abbreviated version on subsequent pages. Numbers in the index correspond to the last two digits of the six-digit CID number.

Contents

Part One

EMERGING FPAs II

ADVANCED HGCDTE FPAs AND APPLICATIONS

IR OPTICS FOR 3RD GENERATION SYSTEMS II

NOVEL UNCOOLED TECHNOLOGIES

INFRARED SEARCH AND TRACK (IRST)-RELATED SYSTEMS AND TECHNOLOGIES

TARGET ACQUISITION SYSTEMS

Part Two

SENSOR VIBRATIONS: SOURCES, EFFECTS, AND ELIMINATION

SMART PROCESSING FOR 3RD GENERATION SYSTEMS

SELECTED APPLICATION PRESENTATIONS I

SELECTED APPLICATION PRESENTATIONS II

SELECTED TECHNOLOGY PRESENTATIONS

Conference Committee

Symposium Chair

Larry B. Stotts, Defense Advanced Research Projects Agency (USA)

Symposium Co-Chair

Ray O. Johnson, Lockheed Martin Corporation (USA)

Program Track Chair

Gabor F. Fulop, Maxtech International, Inc. (USA)

Conference Chairs

Bjørn F. Andresen, Elbit Systems Electro-Optics ElOp Ltd. (Israel)
Gabor F. Fulop, Maxtech International, Inc. (USA)
Paul R. Norton, US Army Night Vision and Electronic Sensors Directorate (USA)

Program Committee

Christopher Carl Alexay, StingRay Optics, LLC (USA)
Raymond S. Balcerak, Defense Advanced Research Projects Agency (USA)
Stefan T. Baur, Raytheon Vision Systems (USA)
Philippe Francois Bois, Thales Research and Technology (France)
Wolfgang A. Cabanski, AIM Infrarot-Module GmbH (Germany)
John T. Caulfield, Cyan Systems (USA)
Jean-Pierre Chatard, ULIS (France)
Peter N. J. Dennis, QinetiQ Ltd. (United Kingdom)
John W. Devitt, L-3 Communications Cincinnati Electronics, Inc. (USA)
Michael T. Eismann, Air Force Research Laboratory (USA)
Martin H. Ettenberg, Sensors Unlimited, Inc. (USA)
Sarath D. Gunapala, Jet Propulsion Laboratory (USA)
Masafumi Kimata, Ritsumeikan University (Japan)
Hee Chul Lee, Korea Advanced Institute of Science and Technology (South Korea)
Paul D. LeVan, Air Force Research Laboratory (USA)
Wei Lu, Shanghai Institute of Technical Physics (China)
Whitney Mason, US Army Night Vision and Electronic Sensors Directorate (USA)
Mark A. Massie, Nova Sensors (USA)
Paul L. McCarley, Air Force Research Laboratory (USA)

R. Kennedy McEwen, SELEX Sensors and Airborne Systems, Ltd. (United Kingdom)
Paul F. McManamon, Air Force Research Laboratory (USA)
John Lester Miller, FLIR Systems, Inc. (USA)
A. Fenner Milton, US Army Night Vision and Electronic Sensors Directorate (USA)
Ofer Nesher, Semi Conductor Devices (Israel)
Peter W. Norton, BAE Systems, Inc. (USA)
Herbert K. Pollehn, Army Research Laboratory (USA)
Ingmar G. E. Renhorn, Swedish Defence Research Agency (Sweden)
Antoni Rogalski, Military University of Technology (Poland)
Myron J. Scholten, DRS Infrared Technologies (USA)
Venkataraman S. Swaminathan, US Army RDECOM-ARDEC (USA)
Meimei Z. Tidrow, Missile Defense Agency (USA)
Philippe M. Tribolet, Sofradir (France)
Jay Vizgaitis, US Army Night Vision and Electronic Sensors Directorate (USA)
Kadri Vural, Teledyne Scientific Co. (USA)

Session Chairs

QWIP, QDIP, DWELL, and QWISP FPAs with Applications
Philippe Francis Bois, Thales Research and Technology (France)
Sarath D. Gunapala, Jet Propulsion Laboratory (USA)

Emerging FPAs I
Meimei Z. Tidrow, Missile Defense Agency (USA)
Venkataraman S. Swaminathan, US Army RDECOM (USA)

Emerging FPAs II
Meimei Z. Tidrow, Missile Defense Agency (USA)
Venkataraman S. Swaminathan, US Army RDECOM (USA)

Advanced HgCdTe FPAs and Applications
Philippe M. Tribolet, Sofradir (France)

Short Wave IR and Applications
Martin H. Ettenberg, Sensors Unlimited, Inc. (USA)

Advanced IR Materials
Christopher Carl Alexay, StingRay Optics, LLC (USA)
Jay Vizgaitis, US Army Night Vision and Electronic Sensors Directorate (USA)

IR Optics for 3rd Generation Systems I
Jay Vizgaitis, US Army Night Vision and Electronic Sensors Directorate (USA)
Christopher C. Alexay, StingRay Optics, LLC (USA)

IR Optics for 3rd Generation Systems II
Jay Vizgaitis, US Army Night Vision and Electronic Sensors Directorate (USA)
Christopher C. Alexay, StingRay Optics, LLC (USA)

Novel Uncooled Technologies
Whitney Mason, US Army Night Vision and Electronic Sensors Directorate (USA)

Infrared Search and Track (IRST)-Related Systems and Technologies
Ingmar G. E. Renhorn, Swedish Defence Research Agency (Sweden)
Gil A. Tidhar, Optigo Systems, Ltd. (Israel)

Target Acquisition Systems
Wolfgang A. Cabanski, AIM Infrarot-Module GmbH (Germany)
Michael T. Eismann, Air Force Research Laboratory (USA)

Uncooled FPAs: The French Connection
Jean-Luc Tissot, ULIS (France)
Whitney Mason, US Army Night Vision and Electronic Sensors Directorate (USA)

Uncooled FPAs and Applications
Stefan T. Baur, Raytheon Vision Systems (USA)
Charles M. Hanson, L-3 Communications Infrared Products (USA)

Sensor Vibrations: Sources, Effects, and Elimination
Alexander M. Veprik, RICOR Cryogenic and Vacuum Systems (Israel)

Smart Processing for 3rd Generation Systems
Paul L. McCarley, Air Force Research Laboratory (USA)
John T. Caulfield, Cyan Systems (USA)

Active Imaging I
R. Kennedy McEwen, SELEX Sensors and Airborne Systems Ltd. (United Kingdom)

Active Imaging II
R. Kennedy McEwen, SELEX Sensors and Airborne Systems Ltd. (United Kingdom)

Advanced FPAs with Selected 3rd Generation Properties
Peter N. J. Dennis, QinetiQ Ltd. (United Kingdom)
Joseph G. Pellegrino, US Army Night Vision and Electronic Sensors Directorate (USA)

ROIC Developments
Paul R. Norton, US Army Night Vision and Electronic Sensors Directorate (USA)

Infrared Activities in Japan
Masafumi Kimata, Ritsumeikan University (Japan)

Selected Application Presentations I
John Lester Miller, FLIR Systems, Inc. (USA)
John W. Devitt, L-3 Communications Cincinnati Electronics, Inc. (USA)

Selected Application Presentations II
John Lester Miller, FLIR Systems, Inc. (USA)
John W. Devitt, L-3 Communications Cincinnati Electronics, Inc. (USA)

Selected Technology Presentations
Michael J. Berger, Elbit Systems Electro-Optics ElOp Ltd. (Israel)

Introduction

The Thirty-Fourth conference on Infrared Technology and Applications was held the week of March 17-20, 2008 at the Orlando World Center Marriott Resort and Convention Center in Orlando, Florida. The agenda was divided into 24 sessions:

1. QWIP, QDIP, DWELL, and QWISP FPAs with applications
2. Emerging PFAs I
3. Emerging PFAs II
4. Advanced HgCdTe FPAs and applications
5. Short wave IR and applications
6. Advanced IR materials
7. IR optics for 3rd generation systems I
8. IR optics for 3rd generation systems II
9. Novel uncooled technologies
10. Infrared search and track (IRST)-related systems and technologies
11. Target acquisition systems
12. Uncooled PFAs: the French connection
13. Uncooled FPAs and applications
14. Sensor vibrations: sources, effects, and elimination
15. Smart processing for 3rd generation systems
16. Keynote: Future Army applications for IR focal plane arrays
17. Active imaging I
18. Active imaging II
19. Advanced FPAs with selected 3rd generation properties
20. ROIC developments
21. Infrared activities in Japan
22. Selected application presentations I
23. Selected application presentations II
24. Selected technology presentations

In addition, there were five poster papers presented for discussion on Tuesday evening. Highlights of each session are noted below. Papers cited are referenced as "-*xx*" where the numbers refer to the paper number in the Proceedings, for example *6940-xx*.

1. QWIP, QDIP, DWELL, and QWISP FPAs with applications

This session covers recent advances in quantum structured focal plane arrays, except for Type II strained layer superlattices that are covered in Sessions 2 and 3. In addition to the reports of detector development, a paper analyzing the potential performance of quantum dot detectors compared with other detectors was presented.

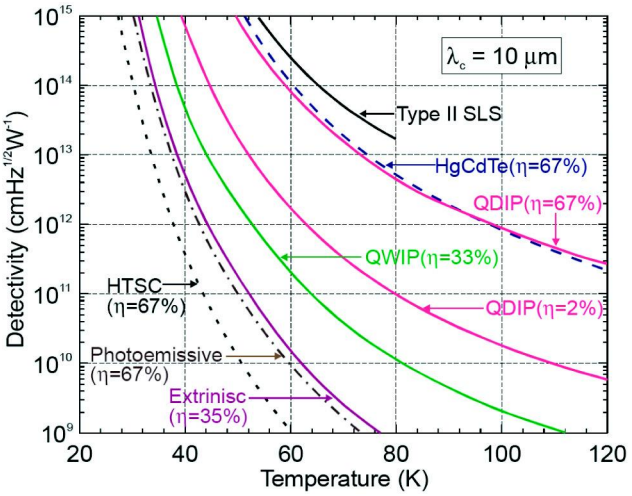

Fig. 1 Theoretical detectivity (D*) for various LWIR (10 µm) detectors as a function of temperature from paper -03. Note the implications of quantum efficiency on the results for quantum dot detectors (QDIPs).

Paper -01 from Acreo and IRnova describes quantum dots deposited in quantum wells (dots-in-a-well or DWELL). The effects of excited states and bias dependence on the spectral response are shown for asymmetrical device structures.

The University of New Mexico reports similar bias-dependence in asymmetrical DWELLs in paper -02. A resonant-cavity structure is used to enhance the LWIR portion of the response. Readout circuit limitations restricted the range of bias that could be applied.

Theoretical comparisons between quantum dot detectors and other types of detectors are presented in paper -03 from the Military University of Technology in Warsaw. Figure 1 illustrates how D* varies with temperature for various detector types. The models and their parameters are summarized and discussed.

Paper -04, presentation only, from JPL described broadband arrays for imaging spectrometer applications. Designs including the use of thin barriers, multiple wells, stacked designs, and intermixing of well depth were discussed, including stackable QWIPs. The potential integration of a QWIP array with an InGaAs was noted.

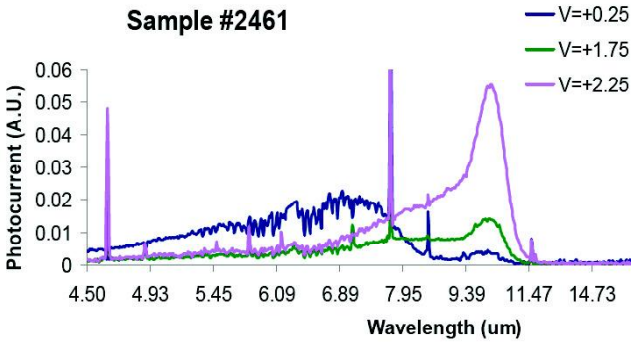

Fig. 2 Bias dependence of Qdot FPA from paper -06.

JPL and the University of Illinois present paper -05 on the potential for far infrared ($\lambda > 30$ µm) or THz arrays based upon quantum well intra-subband photodetectors (QWISP). The authors calculate strong absorption in the far infrared with dopants that couple to the intra-subbands.

Voltage-tunable quantum dots is the subject of paper -06 from the University of Massachusetts, Lowell and Raytheon. Compared to quantum wells, quantum dots are said to have longer lifetimes due to suppressed phonon scattering and longer excited state lifetimes. The bias dependence of the spectral response of a sample FPA is illustrated in Figure 2.

Paper -127 from Thales and Sofradir describes their status of QWIP array development. Two formats are now in production; 384 × 288 and 640 × 512, with 25 and 20 µm pitch respectively. Work on dual-band arrays continues. Also development of polarimetric sensors using a 2×2 polarizing grid metalization mask is described giving ~50 % contrast.

2 and 3. Emerging PFAs I and II

Sessions 2 and 3 contain six papers reporting on Type II superlattice detectors (T2SL), also known as strained-layer superlattices (SLS). These devices are a potential replacement for HgCdTe detectors. Like HgCdTe they have a direct bandgap and a high absorption coefficient α, that allows the detector layer to be thin. Unlike QWIP devices, normally-incident radiation is absorbed, so that grating structures are not needed. The most popular material for making T2SL devices is the combination of GaSb and InAs layers on GaSb substrates. Focal planes in both MWIR and LWIR have been demonstrated in recent years. This session updates the progress in this material system.

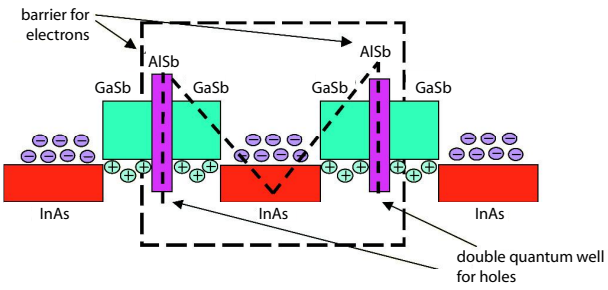

Fig. 3 Type II superlattice "M" structure as described in paper -07 inserts electron barriers to help confine carriers.

Paper -07 from Northwestern University summarized their progress in Type II superlattice detectors. Quantum efficiency of 60-70% is reported after substrate removal. A new structure, named the M-structure and illustrated in Figure 3 is described. Initial results from detectors made in this configuration are reported to give detector impedance (R_0A) of 200 Ωcm^2 for a cutoff wavelength of approximately 10 µm.

Fraunhofer and AIM describe progress in one- and two-color Sb-based superlattices in paper -08. The effect of varying the absorber layer thickness is described on test structures, and for different detector areas. Figure 4 shows a test structure of two-color devices on a 20 µm pitch. Imaging from arrays of two-color MWIR/MWIR in a 288 × 384 format with 40 µm pixels is reported.

Optimal design issues associated with MWIR/MWIR two-color Type II superlattice detectors are discussed by AIM and Fraunhofer in paper -09. This paper summarizes the system-level impacts of higher quantum efficiency and reduced crosstalk that result from increased superlattice layer thickness described in paper -08. The paper also gives a roadmap for future development of large format—640 × 512—single-color MWIR Type II detectors.

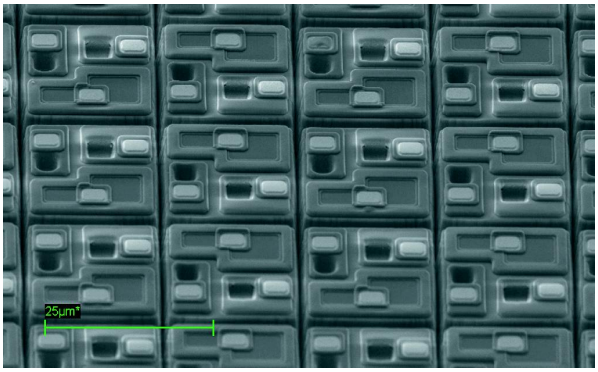

Fig. 4 Two-color Type II superlattice test array on a 20 µm pitch described in paper -08.

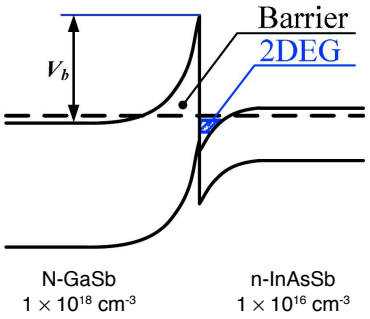

Fig. 5 N-GaSb/n-InAsSb heterostructure interface from paper -11 where 2DEG stands for two-dimensional electron gas.

Paper -10 is presented by JPL and Raytheon describing their work on both LWIR and MWIR Type II SLS detectors. LWIR test structures are reported with R_0A products >5 Ωcm^2 at 80 K for a 12 µm cutoff. Quantum efficiencies of nearly 30 % in these devices gives D* values as high as 8×10^{10} Jones. D* in MWIR devices is reported to be as high as 8×10^{13} Jones for λ_c = 3.7 µm.

Soreq presents paper -11 on heterostructure MWIR detectors based upon MOCVD-grown GaSb/$InAs_{0.91}Sb_{0.09}$ Type II superlattices. The heterostructure is formed in an N-n configuration of InAsSb directly on an n-type GaSb substrate as illustrated in Figure 5. In the usual convention, the capital N indicates the wider bandgap material. Operational theory for this barrier-dominated device is described. Spectral response varies with bias. A device operating with a 4.1 µm cutoff is measured with an R_0A product at 180 K of 180 Ωcm^2.

Paper -12 on nBn (B stands for barrier) Type II detectors is presented by the University of New Mexico, CNRS (France), and QmagiQ. Both MWIR and LWIR devices are described. An FPA fabricated with a 4.2 µm cutoff gives an NEΔT of 24 mK for 16 ms integration time at 77 K with f/4 optics. Two-color operation by reversing polarity is also reported.

4. Advanced HgCdTe FPAs and applications

HgCdTe has established itself as the most versatile detector material for applications that demand the highest performance. It competes with InGaAs in the 1.7 µm spectral range, and InSb in the MWIR, but has no production competition today in the LWIR unless requirements are relaxed to allow for low quantum efficiency. Even after nearly 50 years of development, however, there continue to be challenges faced by those using this material. This session addresses several of these issues as well as new applications.

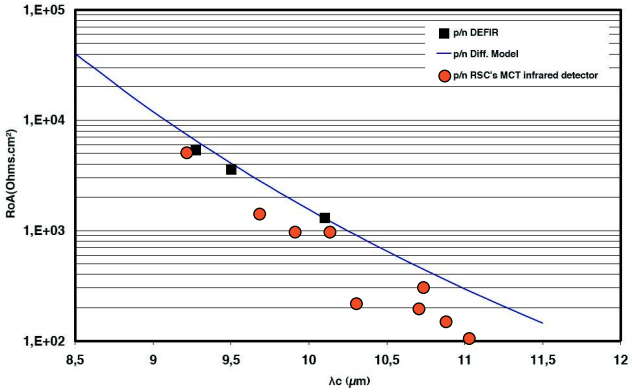

Fig. 6 R_0A product of Defir ion-implanted LWIR diodes from paper -13.

CEA-LETI and Sofradir (Defir) report on MWIR and LWIR As-implanted, p-on-n planar HgCdTe photodiodes in paper -13. Implant defects are reported to be largely removed after the implant activation. R_0A products are comparable to state-of-the-art diodes. LWIR diodes with high reverse breakdown and high R_0A (9.2 µm cutoff, ~1 V, >4000 Ωcm^2) are achieved at 77 K as illustrated in Fig. 6. Quantum efficiency without AR coating is greater than 70% and the diffusion length is approximately 25 µm. Lifetime for minority-carrier holes is 1.8 µsec. Excellent results are also achieved in MWIR material. LWIR and MWIR FPAs with 30 µm pixels have measured responsivity operability of 99.9% and 99.8% with sigma/mean of 4.6% and 4.6%, respectively at 77 K.

Paper -14 from Selex gives their results in the development of LWIR HgCdTe grown on GaAs substrates by MOVPE and its application to multispectral imaging. Multispectral requirements for the LWIR band are discussed, including spectral bandwidth for each subband and the associated signal-to-noise requirements. A six-band filter wheel approach was selected. Results for a 10 µm cutoff array in a 640 × 512 format with 24 µm pixels are described. NEΔT array operability was 99.6%. Estimated R_0A product for the array was 1000 Ωcm^2 making the detectors photon-noise limited under the multspectral application conditions. Trap-assisted tunneling effects are discussed in evaluating diode effects at low flux values.

Maintenance-free reliability of detectors is the subject of paper -15 from Sofradir. Issues discussed include cooler-induced vibrations, vehicle platform vibrations, exposure to high temperature storage, effects of thermal shocks, operating temperature, and vacuum reliability. The impact of ambient temperature on the cooler stability is noted to be reduced by a factor of four when the

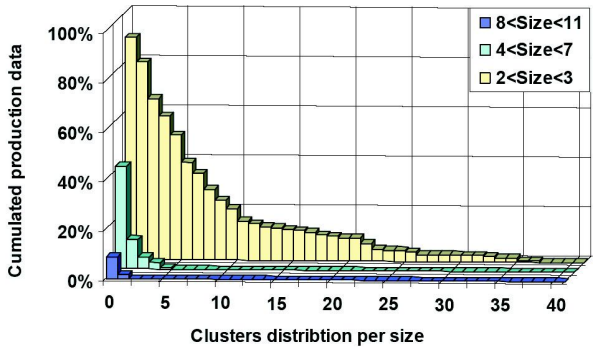

Fig. 7 Cluster-size distribution from 640 × 512 small-pixel (15 µm) MWIR detector production as described in paper -16.

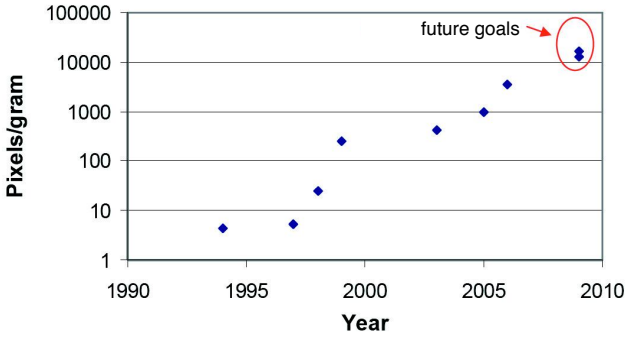

Fig. 8 Trend for InGaAs cameras in the number of pixels per gram of weight from paper -17.

detector operating temperature is raised from 70 to 110 K. HgCdTe FPA reliability is considered with respect to storage, thermal cycling, and operation.

Sofradir discusses the challenges of 640 × 512 small-pixel (15 µm) MWIR detector mass production in paper -16. For this configuration, the cost breakdown is 35% FPA, 20% dewar, and 45% cooler integration and test. Unit to unit response uniformity is <11% and 90% of units have no defect cluster larger than 7 pixels—see Figure 7. LPE production on CdZnTe substrates will be replaced by MBE grown on 4-inch Ge substrates by the end of 2009, reducing chip cost by 20%. 8-inch substrates are planned for the future. Hybridization bump yield is quoted as 99.98%. Readout charge storage is 6.8 or 5.5 × 10^6 e-, depending upon mode—integrate then read, or integrate while read, respectively. Since these devices are strongly background limited, the NEΔT of <17 mK is tightly distributed with a standard deviation of only 4.9%. Operability is typically at 99.98% with a specification limit of 99.5%. Under good atmospheric conditions, the small pixel size gives an ID range of 8.4 km with f/2 optics which is 85% better than for a 30 µm pixel pitch.

5. Short-wave IR FPAs

Development of detectors for the short wavelength infrared (SWIR) band has been very actively pursued for the past several years. They are a potential replacement for image intensifiers under some situations. Other applications in the SWIR include enhanced range for identification and the possibility of range detection through laser radar or range-gated imaging using eye-safe wavelengths. The SWIR region is also of interest for industrial inspection, fused night vision, and astronomy, including SWIR cameras on the Hubble Space Telescope. Astronomers have an intense interest in the development of large format arrays in this spectral region.
Paper -17 from Goodrich describes development of a miniature InGaAs camera without a thermo-electric cooler in order to minimize power consumption when the ambient temperature is high. Progress trends of these cameras with respect to pixels per gram and pixels per W are discussed—Fig 8 shows the trend of pixels per gram. With no temperature stabilization, new algorithms are required to handle nonuniformity correction. The issues involved in operating without temperature stabilization are discussed. Without temperature stabilization the camera does not draw more than about 2 W over the entire -40 to 70 °C temperature range.

Spectrolab reports on very low dark-current InGaAs arrays in paper -18. The array format is 1280 × 1024 with 20 µm pixels evolving to 15 µm pixels in the future. The materials structure is N^+ InP epitaxy on InP substrate followed by a lightly-doped (intrinsic) InGaAs layer and a lightly-doped InP cap layer. Selective Zn diffused diodes are formed that extend through the cap into the InGaAs layer forming a p^+iN diode, as illustrated in Fig. 9. Early experiments identified perimeter-induced leakage currents. With improvements the leakage current is now ~2.8 nA/cm^2. Diffusion lengths of 50-100 µm are reported.

Magnolia Optical Technologies and coauthors consider SWIR imaging in paper -19 using SiGe as the sensor material. SiGe material is already used in some CMOS foundries and can provide spectral response out to 1.6 µm. Modeling of the performance of this material is described. 1.7 µm thick Ge layers grown on Si were evaluated in a *pin* structure. Perimeter leakage is evident,

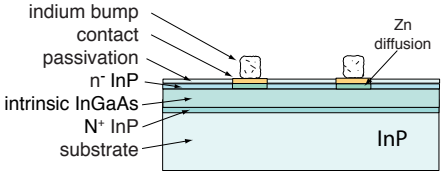

Fig. 9 Epitaxial p+iN+ InGaAs diode as decribed in paper -18.

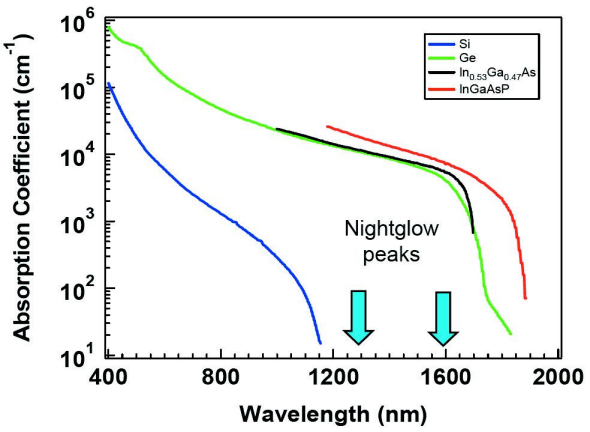

Fig. 10 Absorption coefficient for Si, Ge, InGaAs, and InGaAsP as a function of wavelength, from paper -20.

indicating a need to refine the device passivation.

Paper -20 from NoblePeak Vision reports on the development of monolithic visible-to-SWIR imaging array based upon germanium grown on silicon. The material technology is based upon CMOS foundry processes. Figure 10 compares the absorption coefficients of Ge with Si, InGaAs, and InGaAsP. Dislocation trapping is discussed in the context of reducing the defect density of Ge grown on Si. A monolithic prototype is described with 10 µm pixels in a 128 × 128 format using a CTIA per unit cell and column buffer amplifiers. Performance of the prototype in a camera, including a D* of 2.8×10^{12} Jones, is given.

The final paper, -21, in session 5 was presented by Goodrich on a high-resolution visible/SWIR imager for day/night imaging. The imager format described is 1280 × 1024 with 15 µm pixels using a CTIA readout unit cell with <50 noise e^-, and capable of 120 frames per second in a rolling-frame mode. Total measured noise with the detector was 114 e^- using correlated double sampling (CDS). Response uniformity is measured to be 9% uncorrected. Figure 11 shows an image taken with the imager, after nonuniformity correction.

6. Advanced IR Materials

The selection of IR materials is much reduced compared to the situation in the visible part of the spectrum. In IR dual-band, MWIR/LWIR, systems the selection is further significantly reduced compared to single-band systems. The challenges involved in developing materials for next generation optical systems having requirements for better performance, less weight, volume and cost are addressed in this session.

Fig. 11 Image of the development team of an InGaAs visible/SWIR imager taken by their camera described in paper -21.

Umicore presents in paper -22 a case study where the design of a lens made for automotive applications from their GASIR molded chalcogenide glass material is compared with that of a germanium lens. The GASIR solution is more cost effective because the material may be molded and active or passive athermalisation is not required.

AMTIR is another optical material which is suitable for the molding process. Amorphous Materials summarizes in paper -23 the properties of their molded chalcogenide glass lenses with transmittance from the NIR to the LWIR spectral regions. Antireflection coatings have been developed for coverage of the combined MWIR and LWIR regions.

An innovative dual-purpose black coating—see Fig. 12—is described by Acktar in paper -24. When applied to the inner walls of an IR dewar, the gas-absorbing coating replaces electrical heating-element getters which are required for maintaining a good vacuum. The coating also absorbs infrared stray-radiation and thereby increases detector sensitivity.

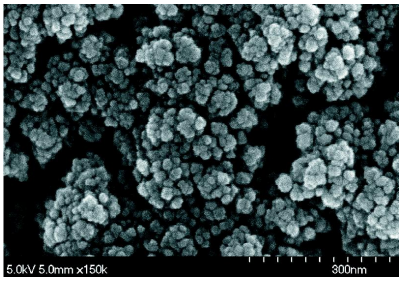

Fig. 12 SEM image of a black coating material that acts as a vacuum getter as described in paper -24.

7 and 8. IR Optics for 3rd Generation Systems

The main emphasis of these two sessions is on the challenges posed by the defense establishment to develop compact 3rd generation optical systems which will answer the requirements for simultaneous system operation in the MWIR and LWIR spectral bands. The enabler is the existence of 3rd generation dual band MW/LW FPAs. Today 3rd generation FPAs also exist with simultaneous passive MW and active SWIR. The new generation of optical systems to support the combination of active SWIR added to the passive dual MW/LW optics, all in one compact system, define the future challenges for the optics designers.

The increased optical complexity involved when advancing from 2nd to 3rd generation FLIRs is discussed by NVESD in paper -25. Among the challenges introduced by simultaneous operation in the MWIR and LWIR bands using common optics are selecting optical materials, implementing dual f-number in the dewar and developing coatings spanning multiple spectral bands.

Rugate Technologies, in cooperation with Corning Specialty Materials and Flemming Tinker, shows in paper -26, by modeling and measurements, that high performance dual band anti-reflection (AR) coatings can be designed and fabricated to performance levels comparable to single band AR coatings. It is concluded that less than 1% reflection in both bands is a realistic goal.

In a follow-up to paper -25, paper -27 from NVESD outlines the motivations for use of 3rd generation technologies in FLIRs and presents the design, fabrication, and testing of their 3rd generation FLIR demonstrator optics—see Fig. 14. The demonstrator shows that a field-ready, small and lightweight imager with exceptional sensor range performance can be quickly realized.

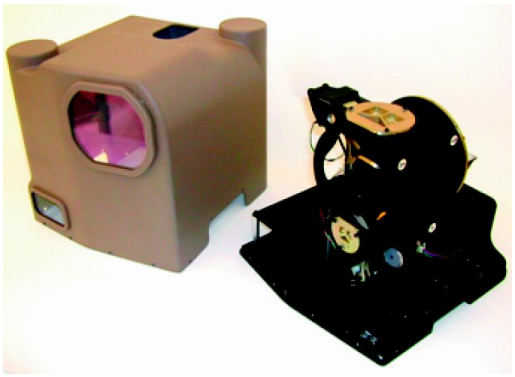

Fig. 14 3rd generation laboratory optics demonstrator from paper -27.

Paper -28 describes Marlow Industries' hermetically sealed thermoelectrically-cooled sources used as reference sources for monitoring the gain and responsivity non-uniformity of FPAs. Typically these sources are mounted in a standard TO-3 or TO-8 packages and swung in front of the FPA during a calibration cycle which may last between 5 and 10 seconds.

MEMS Optical outlines in paper -29 the development of their etching process for producing grayscale IR optics in IG6 ($As_{40}Se_{60}$) substrate material. The process has been used to produce a 16.5 mm diameter diffractive lens. Dual-band color correction for 3rd generation diffractive lenses is discussed in some detail.

A progress report on design, modeling, and fabrication of a miniature IR retroreflector is presented by Pacific Northwest National Laboratory and Dyna Technologies in paper -30. The retroreflectors, required to have large acceptance angles and efficient returns, have several applications in defense and optical communications.

The challenge addressed by TelAztec in paper -31 is the design and fabrication of an antireflection treatment for the substrates of back-side irradiated HgCdTe FPAs in space. The company has demonstrated that the incorporation of substrate surface relief microstructure arrays provides excellent optical performance, radiation hardness and environmental durability.

KiloLambda discusses their novel wide-band threshold-triggered protection filter in paper -124. The blocking response time is in the nanosecond range. The blocking is presently non-reversible and leaves an opaque spot the size of a pixel where the intense radiation impacts the filter in the image plane.

Paper -32 describes the efforts at Resonon to develop a compact hyperspectral imaging sensor for a small unmanned aerial vehicle (UAV). Fig. 15 shows an outline of the design characteristics of the new anamorphic im-

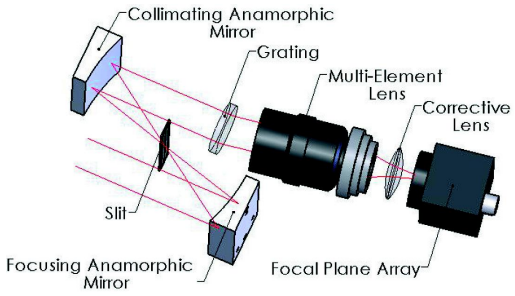

Fig. 15 Anamorphic optics focus only along the spectral axis with no effect on the spatial axis—from paper -32.

aging spectrometer that is described in the paper. The design concept benefits from a reduction in complexity over standard high-performance spectrometer optical designs.

9. Novel Uncooled Technologies

One of the paths to improved microbolometer thermal sensitivity is through higher temperature coefficient of resistance (TCR) bolometric films. Paper -33 from Univ. of Missouri/Columbia describes the deposition of $Si_xGe_{1-x}O_y$ thin films with varying stoichiometries by RF magnetron sputtering. The highest value of TCR obtained at room temperature is 5.8 %/K, which is more than double that typically obtained with VOx and amorphous silicon thin films.

In paper -34 Agiltron describes a 280 × 240 dual-band (MWIR/LWIR) uncooled bi-material microcantilever IR sensor with an optical readout. In addition, a noise model is presented for the uncooled imager and compared to modeled cooled InSb and HgCdTe FPAs. It is claimed that, by increasing the responsivity of the uncooled sensors, the shot noise could be minimized to such an extent that the sensor could outperform the cooled sensors at both cryogenic and room temperatures. However, no experimental verification for this claim is given and the only images shown are of a Bunsen burner.

Multispectral Imaging in paper -35 describes progress in fabricating bi-material microcantilever FPAs that are read out by changes in capacitance. The company has demonstrated 160 × 120 arrays with 50 µm pixels, with the best NEΔT achieved being 40 mK at an FPA temperature of –19 °C. Figure 16 shows the arrangement of their thermally-compensated pixel. Uniformity continues to be an issue but transfer to a more controlled production environment is expected to result in further improvement.

In paper -36 another capacitive bi-material microcantilever FPA is described by KAIST (South Korea), with an electrically floating top plate and improved fill factor.

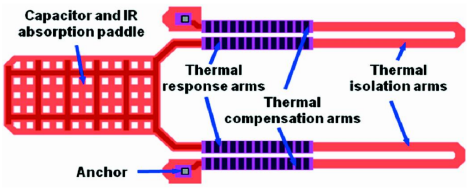

Fig. 16 A thermally-compensated microcantilever pixel described in paper -35

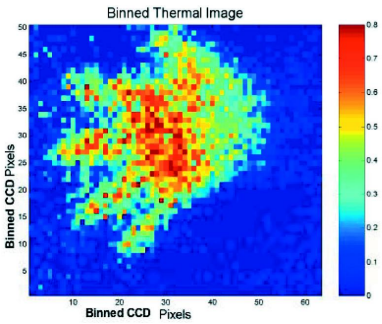

Fig. 17 Image of a hand, made with a 50 × 64 TVT array from paper -37

Paper -37 from Science Research and CNRI MEMs Exchange presents a thermal-to-visible transducer (TVT) based on tiny Fabry-Perot Interferometers (FPI) at each pixel. The optical transmission (to a probe NIR laser beam) of the FPIs is temperature dependent and is read out by a CCD or CMOS camera. An image taken with a 50 × 64 array is shown in Fig. 17. However, further progress requires the deposition of a highly reflective film on the infrared-absorbing polymer film.

Paper -38 from Redshift Systems presents the latest results in developing a Thermal Light Valve™ (TLV) FPA, whose principle of operation is based on the changes in reflectivity of a temperature-sensitive thin film filter. The reflectivity changes are sensed by a near-infrared (NIR) probe beam and are imaged by an off-the-shelf CCD or CMOS imager. An 80 × 60 array is shown to have an NEΔT of 174 mK.

Carbon nanotubes (CNTs) have outstanding electronic properties, such as 1-D near ballistic transport, lack of surface dangling bonds, low thermal noise and chemical robustness. In paper -39 from Michigan State, bandgap engineering of CNTs is discussed and the construction of a CNT of the appropriate bandgap for infrared absorption is demonstrated.

10. Infrared Search and Track (IRST)-Related Systems and Technologies

This session discusses target search and track systems for short ranges, typically 100 meters, as well as for ranges longer than 10 km. The short range systems have a FOV ranging from a sphere to nearly a hemisphere while the long range systems are panoramic and cover typically 5 – 20 degrees in elevation near the horizon.

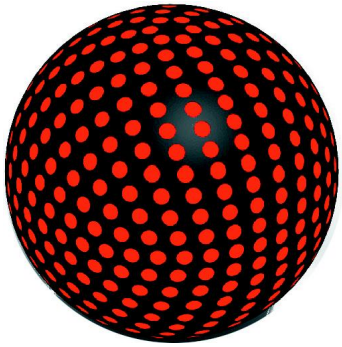

Fig. 18 The Spherical Sensor Configurations (SSC) concept from paper -41 where each red spot represents an individual sensor.

The problem of detection and tracking of targets at ranges from a few tens to a hundred meters over a 4π FOV is discussed by Lucid Dimensions in paper -41. Sensors are distributed over a sphere and the target coordinates are determined by comparing the signals from the different sensors—as illustrated in Fig. 18. A 2D prototype having 30 sensors is demonstrated.

In contrast to the previous paper, ImmerVision's concept, outlined in paper -42, is to use one large FPA and a panomorph lens to cover a hemispheric field of view. This type of lens is a particular design form of a wide angle lens. Optical distortion is controlled in order to increase situational awareness in zones of interest.

A 3rd generation high-performance naval MW IRST system is described by Sagem DS in paper -43. The system head performs a continuous panoramic scan while a counter-rotating training scanner provides a stepped freezing of the FOV direction during the short staring period of the large FPA. Figure 19 shows the optics layout of their IRST.

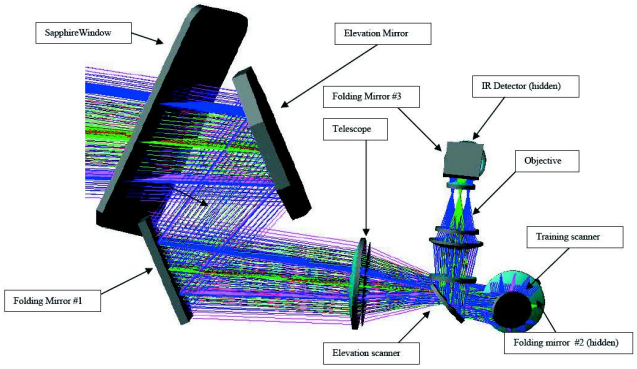

Fig. 19 Optics layout of the VAMPIR NG IRST as discussed in paper -43. The training scanner is found in the lower right-hand corner.

A Distributed Aperture System, DAS, for the U.S. Navy was the subject of NRL's "presentation only" -44. Eight MWIR imagers are positioned along the ship's periphery. With two FOVs the IRST system is optimized for both missile detection and asymmetric situational awareness operation. A 512 × 2560 elements HgCdTe FPA is used with a 30 Hz frame-rate. The resulting elevation IFOVs are 0.1 mrad and 0.3 mrad, respectively for the two modes. Videos from field testing were shown.

"Presentation only" paper -45 from L3-Cincinnati Electronics discussed recent results, current efforts, and future directions in their development of a new generation of extremely large format IRFPAs—see Fig. 20. 4K × 4K InSb with 15 μm pitch is in fabrication, 6K × 6K with 10 μm pitch is proposed for next year and an 8 μm pitch Giga-pixel FPA is set as a goal for realization within the next five years. In the LWIR region a 1K × 1K C-QWIP FPA has been flown while a 2K × 2K FPA is at the planning stage. Among other emerging concepts that were mentioned are pixel level micro-polarizers, two-color pixel filters in a checkerboard pattern, and a micro-lens array imager which promises reduction in volume, mass and cost with vast simplification of optics.

As naval operations against asymmetric threats in coastal areas are assuming an increasing challenge, the understanding and modeling of IR system performance in these complex environments are becoming critical to successful design of IRST systems. TNO reports in paper -46 on their measurements on "dc" background, clutter, and a target in bay environments. The measurement data is used to extend the usefulness of their "open sea" prediction models to include coastal areas.

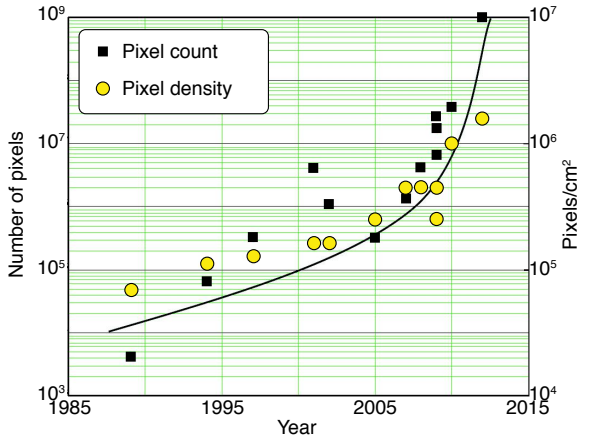

Fig. 20 Measured and predicted InSb FPA format and pixel density from presentation -45. Notice the Giga-pixel predicted for 2012!

A concept for a dual band, MW – LW, shipborne IRST system is presented by Samsung Thales in paper -115. Adaptive temporal and spatial filtering techniques are used for clutter reduction and an extended Kalman filter together with an integrated probabilistic data association algorithm are adapted for target tracking. The system is of the scanning type with two 480 elements linear array detectors and 6 elements in TDI. A next-generation system using a 2D FPA is envisaged.

11. Target Acquisition Systems

The span of target ranges considered in this session is enormous – from space to less than a meter. The majority of the papers are concerned with protection of soldiers from poisonous gases, explosives, and gun fire—from enemy as well as from friendly forces.

A miniaturized IRST-type system for operation at ranges up to 200 meters during asymmetric warfare is demonstrated by Carl Zeiss Optronics in paper -47. The system, which consists of a daylight camera and a thermal imager with a 640 × 480 α-Si microbolometer FPA, is designed for target acquisition from a stabilized platform mounted on a vehicle in motion.

The question being asked by Elbit/ElOp in paper -48 is whether a low-light-level, EMCCD, visible, or an MWIR channel is optimum for spaceborne low-Earth-orbit night imaging. It is shown by theoretical analysis that the performance of the cryogenically cooled IR channel with 32 elements in TDI is superior to a low-light-level visible channel with 128 elements in TDI also under full moon conditions.

Paper -49 from Carl Zeiss Optronics addresses the IR/EO system requirements of the future land warrior. Their Opus-H light-weight hand-held navigational and targeting devise consists of a NIR camera for target identification, an uncooled LWIR thermal camera for observation and a direct view visible channel, in addition to LRF, GPS and a digital compass. Typical identification ranges against a standard NATO target are given as 2.5 km and 1.0 km, respectively for the NIR and LWIR channels.

Protection of the soldier against poisonous gases, explosives and gun fire is the subject of AIM Infrarot-Module in paper -50. Gas identification is carried out by a UAV-mounted hyperspectral imager. A tunable laser in combination with a broadband HgCdTe FPA-based thermal imager detects explosives via analysis of backscattered

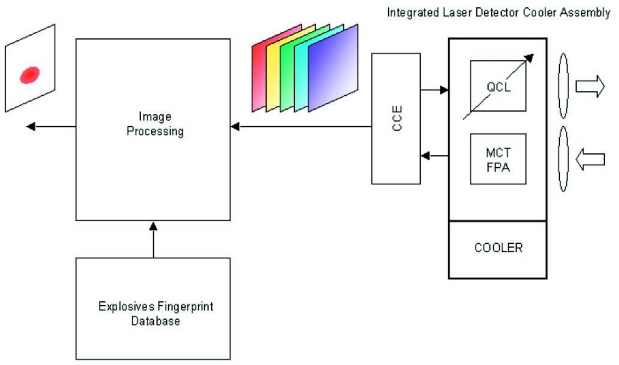

Fig. 21 Concept of laser stimulated IR imaging spectrometer for detection of explosives in paper -50.

spectral images—see Fig. 21. AIM's HuntIR sight is trained on the gunflash source after an acoustic sensor accurately determines the direction to the threat.

Helmut-Schmidt University reports in paper -51 on their efforts to dramatically increase the hit probability of light weapons. They have, in cooperation with AIM, developed fire control algorithms for integration into existing TWS digital signal processors. The success of the resulting fire control computer was demonstrated with the RangIR weapon sight mounted on a grenade machine gun.

A new concept and algorithm for automatic scene construction from aerial infrared imagery—illustrated in Fig. 22—is proposed by FGAN-FOM Research Institute for Optronics and Pattern Recognition in paper -52. The work was undertaken in order to overcome the problems due to occlusion or jamming of GPS in warfare conditions. The 3D reconstruction from 2D image sequences is based on Computer Vision's SfM, Structure from Motion, technique. Navigation and target identification are the most important applications.

Advantages of the SWIR spectral band for acquisition of high temperature transient events like gun muzzle flashes is discussed by Optigo in paper -53. It is claimed that this band is optimal for the search, detect and track system. A dual band SWIR – NIR/VIS high frame rate camera engine has been demonstrated.

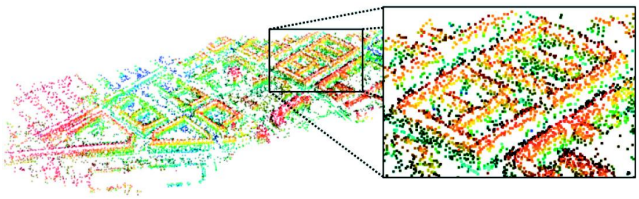

Fig. 22 Illustration of the navigation method discussed in paper -52.

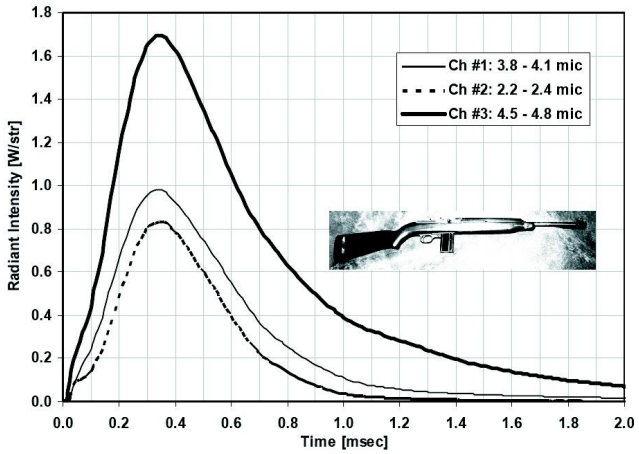

Fig. 23. Muzzle flash radiant intensity from a M1 rifle. From paper -55.

Another muzzle flash detection system operating at the lower end of the IR spectrum was presented by the Missile Department of the Israel Defense Forces in paper -54. The omni-directionally staring system is based on low-cost off-the-shelf CMOS cameras and newly developed spatial and temporal algorithms for separation of flash signals from false alarms. A model is presented for the sun glint signals due to sensor motion. It has been experimentally validated using a fast frame camera installed on a truck in various scenarios including desert, forest and urban areas.

In order to design the above systems for detection of transient threats, the flash's spectral and temporal behavior must be measured. IARD, Institute for Advanced R&D, describes in paper -55 a method for utilizing a fast four-channel radiometer to extract the source characteristics. Measured intensity vs. time for the muzzle flash of the M1 rifle is shown in Fig. 23.

The next two papers address standoff detection of chemical and biological agents, as well as targets, by use of hyperspectral imagers. The U.S. Army Research Laboratory reviews in paper -56 progress in developing compact systems based on several technologies. They report on field measurements which show that detection of camouflaged targets may be greatly improved by combining hyperspectral and polarization sensing.

In a companion paper, -57, Pacific Advanced Technology discusses the difference in performance of two hyperspectral imagers, based on diffractive optics technology, when tuned to 10.3 μm and viewing difloroethane and trichloroethane gases . One imager is equipped with a QWIP FPA and the other with a HgCdTe array. The better performance of the QWIP-based imager is believed to be due to less stray background radiation in the 0.5 μm bandwidth system.

Bethel University, in cooperation with AFRL, describes in paper -58 a high resolution imaging spectrometer with simultaneous operation in two bands, MW and LW. A grating is used as the dispersive element and the wavelength resolution was found to be 0.024 μm and 0.083 μm, respectively in the two bands. The 1st and 2nd orders of diffraction, which simultaneously impact the detector, are separated by the dual band FPA. The use of a prototype system for temperature measurement of a 423 K blackbody is demonstrated.

A novel technique of NIR imaging is presented by University of Warwick in paper -129. The technique, which has great potential for homeland security applications, is based on the fact that photons in the 0.7 – 0.9 μm band transmit well through clothing, plastic, paper, water and biological tissues. It may be used for stand-off detection of explosives, drugs and chemical hazards. The proposed system is simple and inexpensive. A conventional LED source, like a TV remote controller, is sine wave modulated and detected by a photodiode and a lock-in amplifier—see Fig. 24.

The ratio of deaths by friendly fire to deaths by enemy fire in wars has always been unacceptably high. The identification-friend-or-foe, IFF, system concept presented by Xiamen University in cooperation with Vestfold University College in paper -116 is based on a MEMS IR array emitter modulated at 30 Hz. The design, fabrication and characterization are described in some detail.

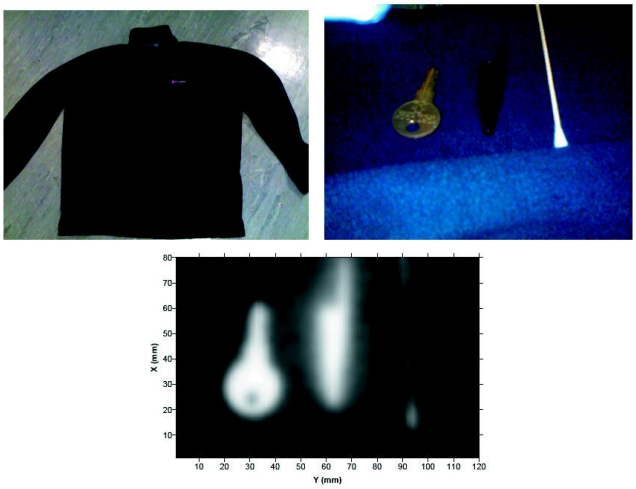

Fig. 24. Lock-in NIR imaging through a garment reveals different obscured objects. From paper -129.

12. Uncooled FPAs – The French Connection

Uncooled FPAs are of enormous interest to the community. Sessions 12 and 13 contain papers on this important subject. Session 12 includes the status of uncooled amorphous silicon technology in France at CEA LETI-LIR and ULIS. Session 13 contains other uncooled papers.

Tremendous progress has been made since this technology development began in the late 1970s. Today, large-format arrays are available from a number of sources with 25 µm pixels. The trend towards ever-smaller pixels continues as well, along with the drive to add features, reduce cost, and expand applications.

ULIS and the Université Paris Sud report in paper -59 on design trade-offs for incorporating analog-to-digital converters (ADC) into uncooled detector readouts. They conclude that a pipeline architecture with 14 bits is possible for small arrays, such as 160 × 120, while larger formats, such as 640 × 480, require ADCs in each column with a dual-ramp feature.

High-end applications using a ¼ VGA (384 × 288) format with 25 µm pixels is discussed by ULIS in paper -60. NEΔT in the range of 30 mK (f/1, 300 K, 60 Hz)—see Fig. 25—is reported with a time constant of 7.7 msec. Operability is routinely >99.99%.

Paper -61 describes progress in moving from 35 µm pixels to 25 µm and then to 17 µm pixels. 25 µm pixel figure of merit (FOM) are reported to be 285 mK msec in production and as low as 166 mK msec in laboratory prototypes. Recently, a 1024 × 768 α-Si microbolometer was fabricated with an NEΔT of 85 mK. Further improvements are expected to result in a 1024 × 720 array with NEΔTs less than 40 mK.

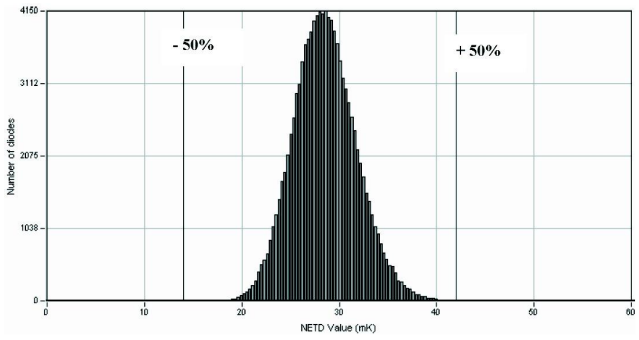

Fig. 25. NEΔT distribution of 25 µm pixels from a 384 × 288 uncooled FPA as presented in paper -60.


Fig. 26. Image taken with a 1024 × 768 α-Si microbolometer with 17 µm pixels as decribed in paper -62.

The development and testing of a large-format, 1024 × 768, α-Si microbolometer with single-level 17 µm pixels is reported by ULIS in paper -62. Figure 26 shows an image from one of these uncooled arrays. This large array uses two analog outputs and operates at 25 frames per second. Faster frame rates are available on a windowed portion of the array. High response uniformity, σ/m as low as 1.7 %, and high operability, >99.99 % are reported. Currently with a 6 msec time constant, the sensitivity or NEΔT is 85 mK with plans to reduce this <40 mK.

Paper -63 from CEA-LETI outlines a wafer-level vacuum packaging technique—called Monolithic Micro Capping (M2C)—for microbolometers, which relies on an infrared-transparent thin film for the cap. The technique has been applied to 25 µm α-Si microbolometers. Since residual pressure is still too high, additional desorption methods are being investigated.

The development of a TEC-less 384 x 288 (25 µm pixels) a-Si microbolometer is reported in paper -64 from ULIS. Instead of using the interpolation of the gain and offset tables obtained at various focal plane temperatures during calibration, the nonuniformity correction method interpolates the DC output voltage tables.

13. Uncooled FPAs

Paper -65 outlines SCD's improvements in its VO_x microbolometers, including development of a 640 × 480 array with 25 µm pixels. The arrays feature variable gain to provide a high dynamic range mode, NEΔT <50 mK (f/1, 60 Hz), and TEC-less operation. Future plans are also discussed.

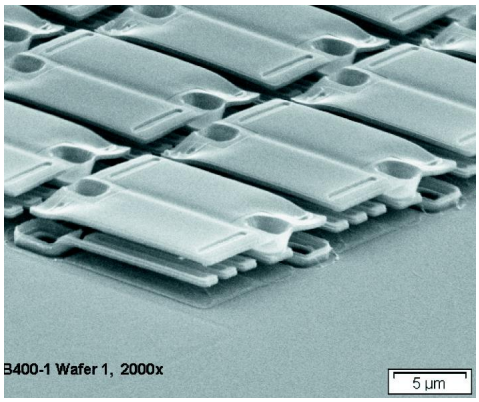

Fig. 27 SEM of 640 × 512, 17 µm two-level microbolometer FPA pixels from Raytheon paper -67

BAE Systems' 640 × 480 VO_x microbolometers on a 17 µm pitch is presented in paper -66. The company has also developed a short time constant version of this microbolometer by adjusting the microbridge leg width and bridge nitride thickness. This version has a time constant of 5 ms and an NEΔT of <100 mK.

Development of an athermal (TEC-less) 640 × 480 uncooled sensor with a unit cell size of 17 µm × 17 µm, and performance approaching that of the 25 µm arrays is reported in paper -67 from Raytheon. Fig. 27 shows an SEM of the 17 µm pixel. Athermal operation is achieved by a combination of dynamic biasing of the array while imaging, coupled with an additional "per pixel" digital correction.

Paper -68 presents the development at L-3 Infrared Products of 17 µm α-Si microbolometers in formats of 320 × 240, 640 × 480, and 1024 × 768. The use of α-SiGe bolometric films has shown TCR of up to 5 %/K and reduced 1/f noise as illustrated in Fig. 28.

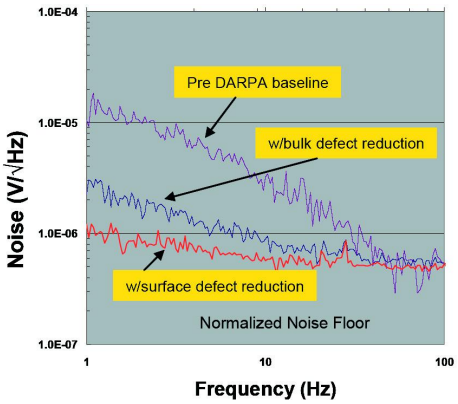

Fig. 28 Improvements in microbolometer bulk and surface properties described in L-3 paper -68 lead to reduction in 1/f noise.

A low-cost passive IR (PIR) security sensor is described in paper -70 from Electro-optic Sensor Design. This sensor employs a mosaic pixel FPA (MP-FPA) in which each pixel comprises a number, N, of sub-pixel microbolometers connected in parallel. The pixel resistance is thus 1/N that of the sub-pixel detectors. It can be shown, and has been confirmed by experiment, that both Johnson and 1/f noise of the pixel are reduced by a factor 1/N that of the individual detectors. A new FPA design offers the potential for an NEΔT of ≤100 mK for packaging in nitrogen at atmospheric pressure. The detection range for human targets is 2 to 5 times greater than for current production sensors.

Paper -71 from L-3 Infrared Products presents the development of Thin Film Ferroelectric TFFE FPAs which have now reached performance (NEΔT) levels of 80 – 90 mK with 48.5 micron pixels. However, these FPAs face the challenge of catching up with microbolometers having ever smaller pixels sizes

Two new low-power approaches for reading out uncooled microbolometers are proposed in paper -72 from the Middle East Technical University. In the first method the readout channel array is separated into groups in order to decrease the load capacitance seen by the readout channel output—see Fig. 29. In the second method, a special op-amp architecture is utilized where the output current driving capacity can be digitally controlled. Simulations show that using these methods results in a power dissipation reduction of 80% and 91% for the readout channels optimized for a single output 384 × 288 FPA operating at 25 fps and for a two-output 640 × 480 FPA operating at 30 fps, respectively.

Paper -122 from Middle East Technical University reports on a new method for estimating the absorption characteristics of uncooled infrared detectors. The method makes use of the Cascaded Transmission

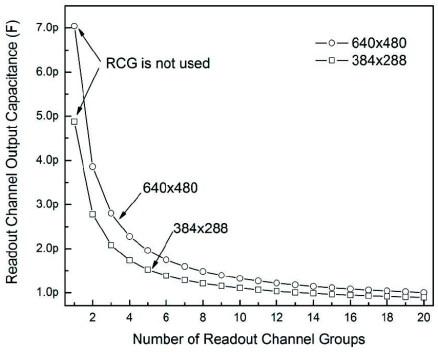

Fig. 29 Capacitance reduction by the method described in paper -72 leads to reduced power consumption by the readout.

Line (CTL) method but can handle microbolometer structures having many different layers and regions. The total absorption can be estimated and optimized by calculating the weighted average of the absorption coefficients of the individual regions with respect the occupied area in the detector.

Middle East Technical University in paper -123 describes an optimum reference detector design for resistive microbolometers. The design is based on a number of rows of nearly infrared-blind elements which cancel the bias heating of the active elements. Simulation shows that the technique cancels 87% of the bias heating effect.

Paper -118 from KAIST proposes a CMOS readout IC (ROIC) that also provides pixel-level analog-to-digital (ADC) conversion for 320 x 240 microbolometers. The proposed ROIC would improve performance and reduce system cost and power consumption. The noise performance of a microbolometer is improved by using the pixel-wise readout structure because integration time can be increased up to 1 ms.

14. Sensor Vibrations: Sources, Effects, and Elimination

Paper -73 from Loughborough University is concerned with elimination of audible noise from the cooler of a high-performance portable IR imager. The noise may lead to a premature detection when the imager is in close proximity to the target and when high-sensitive acoustic equipment is used by the opponent force. This paper uses finite element modeling approaches to achieve the optimal design of vibration protective pads. Measurements have validated the theoretical findings.

The reduction of vibration transfer from a dynamic environment to a gyrostabilized IR/EO payload is the subject of paper -74 by Ricor, Rafael and Lougborough University. An enhanced dynamic model of a snubbed vibration isolated payload comprising an IR sensor is presented. The model is used in the design of the optimal snubbers.

Ricor describes in paper -125 their approach to the redesigning of a Stirling cryogenic refrigerator for use in vibration-sensitive electron-microscopy where the image resolution is specified in angstroms. The objective was achieved by use of passive mechanical counterbalancing in combination with an active two-axis control of residual vibration.

15. Smart Processing for 3rd Generation Systems

Smart, on-focal-plane signal processing becomes increasingly important as FPA size and sophistication increases. Smart processing in the analog mode, or in a combination of analog and digital within the FPA mimics signal pre-processing functions in biology. The functions done before signals are sent to a system signal processor can save power and capture important information in an efficient way. In some cases smart processing can also greatly reduce the data stream sent off the focal plane, making the system much more efficient. This session contains papers that address the motivation and the development of these important functions.

The inspiration derived from biological signal processing, particularly in the retina and near-retinal region, was the topic of the lead-off paper -128 (presentation only), from Eglin Air Force Base.

MDA and AFRL in paper -75 describe the integration of an IR focal plane with a massively parallel processor—a cellular neural/nonlinear network, or CNN. The network can process up to 10,000 frames per second, an important factor when dealing with fast-moving objects. The work reported in this paper concerns integrating the CNN processor with an InGaAs SWIR sensor using indium bump hybridization.

High-speed image-flow processing is the topic of paper -77 from AnaFocus. CMOS circuitry is employed to accomplish this objective while using biologically-inspired parallel and concurrent functions in analog, such as bandpass filtering.

Polaris presents paper -78 on image processing techniques for single-frames of low signal-to-noise (1.25-3) imagery. Fig. 30 shows the probability of detection vs. signal-to-noise for various algorithms described in this

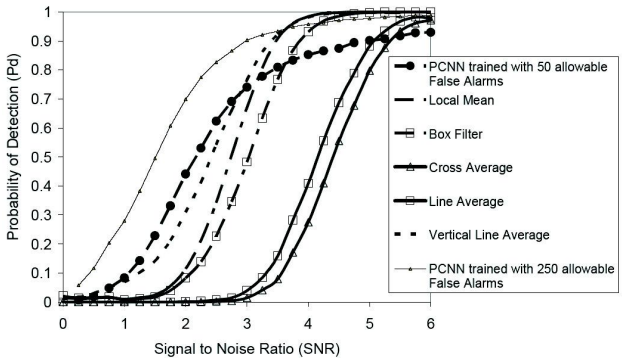

Fig. 30 Single-frame probability of detection for a variety of algorithms described in paper -78.

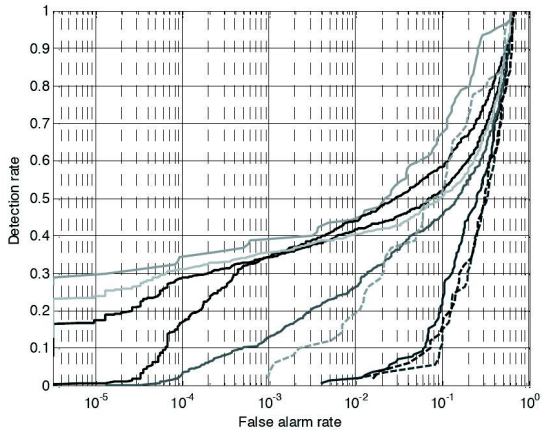

Fig. 31 Detection vs. false alarm rate from paper -79 for nine targets in a study using multispectral data.

paper. Even with such marginal data, the probability of detection can be as high as 95 % when used with pulse-coupled neural networks and filters to separate signals from noise.

Paper -79 presented by the Swedish Defence Research Agency addresses the target discrimination using hyperspectral and multisensor data. 240 spectral bands are segmented into background classes and optimal band selection is discussed depending upon the target. Fig. 31 shows an example of the detection vs. false-alarm rates for nine targets.

Robotic applications of vision sensors arrays was the topic of paper -126 (presentation only). The focus of interest for the applications is robotic flight issues such as obstacle avoidance and position-holding. Relatively small array formats and high frame rates are features of the examples covered.

The final paper of this session, paper -81, addresses the use of a high speed MWIR reference source for non-uniformity correction. Negative luminescence in HgCdTe diodes provide the features used in this application and their high speed allows for multiple temperature calibration. Challenges faced are the relatively large drive currents of 1-2 A/cm^2 for the devices.

16. Keynote session—Future Army applications for IR focal plane arrays

This presentation-only talk, paper -82, reviewed the applications that the Army sees for future infrared FPAs. The topics covered were pilotage and distributed aperture sensors, dual-band for extending detection and identification ranges, SWIR arrays as a possible replacement for image intensifiers, airborne persistent surveillance over battlefields, and vehicle needs for threat warning. In order to address these applications, cost reduction tasks are important, such as large-area substrates for HgCdTe growth and higher performance uncooled arrays.

17 and 18. Active Imaging I and II

Active imaging systems are growing in interest because they offer the possibility of longer range identification and also 3D imaging. The technology is mainly based on HgCdTe with two varieties—n-type MWIR material that can operate cooled as a thermal imager and at higher bias as an electron-avalanche photodiode array—and p-type SWIR HgCdTe that operates at room temperature as an avalanche photodiode. Reports on progress with both varieties are covered in these sessions.

Paper -83 from Selex describes the combination of active and passive imaging with an MWIR (4 μm) HgCdTe array in a 320 × 256 array with 24 μm pixels. In the avalanche mode a gain of 50 is achieved at 6.5 V bias. Higher gains are now reported. Relative insensitivity of range accuracy as a function of range gate is noted—see Fig. 32. Cameras with 3D imaging are being developed with the ability to image people at 15 km and ships at 50 km.

LETI presents their progress towards developing 3D ladar imaging readout circuits in paper -84. They use MWIR n-on-p avalanche photodiodes with gain >20 at 5 V bias. Using a demonstration array in a 10 × 10 format having 40 μm pixels, both capacitive-feedback transimpedance amplifier (CTIA) and buffered direct injection (BDI) circuits were built and tested.

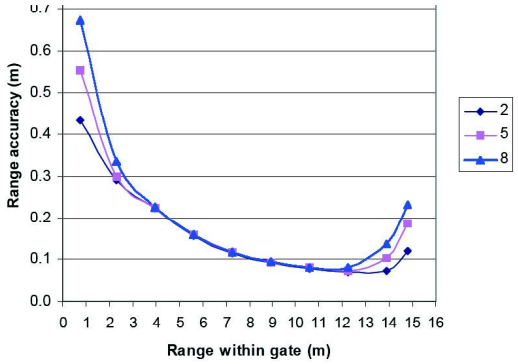

Fig. 32 From paper -83 showing the small dependence of range accuracy on the laser pulse width—numbers in nsec.

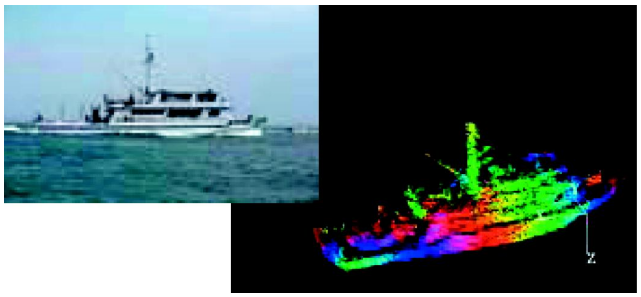

Fig. 33 Ladar image (right) of a ship (left) taken at a range of 2 km with a linear array of APD sensors—from paper -86.

The development of MWIR HgCdTe avalanche photodiode technology is reported in paper -85 by LETI. HgCdTe grown by both MBE and LPE with spectral response out to ~5 µm is used. Very high gain devices are reported—200 at 8 V bias. In video mode at f/4 the NEΔT values are 12 mK with 99.9 % operability. With APD mode gains up to 100 the excess noise factor is reported to be <1.2. Carrier diffusion gives a impulse response time of several nsec.

Paper -86 from Raytheon reports on the development of 3D ladar sensors using HgCdTe and InAlAs avalanche photodiodes. 3D images have been demonstrated with earlier versions of this technology using linear arrays—see Fig. 33. Progress on the latest sensor technology using an 8 × 8 array is reported. This array has bandwidth in excess of 1 GHz and with an NEI < 0.5 photons the sensor is capable of single photon detection. SiGe is used in the readout and the detectors operate in a linear mode with gain >60.

19. Advanced FPAs with Selected 3rd Generation Properties

Dual-band detection was the main focus of this session. These sensors are capable of detecting in two spectral regions simultaneously, or near-simultaneously. This ability allows for unique and compact systems where exploitation of two bands from a single sensor allows the user to gain new advantages in tactical situations.

Sofradir and LETI describe their MBE-grown HgCdTe dual-band development progress in paper -87. They are using an n-on-p pseudo-planar pixel approach as shown in Fig. 34. Currently a MWIR/MWIR 640 × 512 format array is being developed with 24 µm pixels. Work is described in preparation for a transition to smaller pixel sizes.

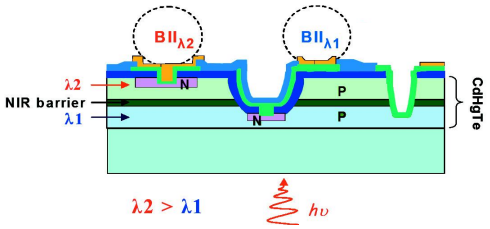

Fig. 34 Schematic cross section of psuedo-planar dual-band pixel—from Sofradir and LETI—paper 87.

Paper 88 from QinetiQ summarizes their work on MWIR/LWIR dual-band HgCdTe arrays grown by interdiffused, multilayer MOVPE on Si substrates. Using a back-to-back diode design with a single indium bump, arrays are fabricated in a 320 × 256 format with 30 µm pixels. The readout has two capacitors for storing charge from each band with capacities of 7.6×10^6 e^- in each and gave NEΔT values of 17 mK for the MWIR band and 33 mK for the LWIR band at f/2.3. The operability of the arrays is reported to be 99.4 and 98.2 % for the MWIR and LWIR bands respectively.

A dual-band MWIR/LWIR HgCdTe sensor engine is described by Raytheon in paper -89. The dewar-electronics module is the size of a Campbell's soup can—4.75 × 2.25 × 1.75 inches—see Fig. 35—and provides a 14-bit digital signal to the image processor. The dewar includes a variable rectangular f/stop mechanism. The sensor engine electronics offer either 2-point nonuniformity correction, or scene-based correction along with scene enhancement.

Selex writes about dual-band MWIR/LWIR HgCdTe FPAs grown by MOVPE in paper -90. Growth on GaAs substrates as large as 6 inches is planned. Using a 640 × 512 format with 24 µm pixels the MWIR, NEΔT has been measured at 14 mK with operability of 99.6 % and 23 mK in the LWIR band with operability of 99.9 % when the bands are operated independently. When operated

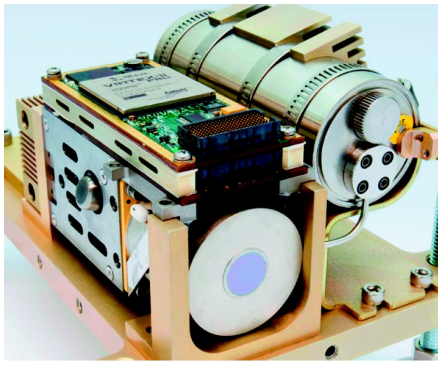

Fig. 35 Dual-band MWIR/LWIR HgCdTe sensor engine (FPA, dewar, electronics, and cooler) —from paper -89.

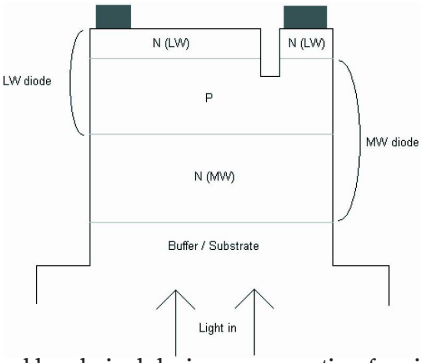

Fig. 36 Dual-band pixel design cross-section for simultaeous detection—from paper -90.

in dual-band mode the NEΔTs were 24 and 26 mK for MWIR and LWIR respectively. The design of a pixel for true simultaneous operation is illustrated in Fig. 36.

Paper -91 from JPL reports on a megapixel dual-band MWIR/LWIR QWIP focal plane array. After describing the individual bands separately, the results from the stacked dual-band pathfinder 320 × 256 FPA with 40 µm pixels are covered, including the device structure (2- and 3-bump versions), spectral response, image examples, and NEΔT measurements. The paper concludes with a description of the initial fabrication of a full 1024 × 1024 format device.

The final paper, -92, of Session 19 is from SCD and describes barrier photodetectors that are designed to eliminate carrier depletion in the narrower bandgap detection region, thus removing generation-recombination leakage currents due to that effect, leaving only diffusion current sources. This should extend the diffusion-limited performance to lower temperatures, allowing higher temperature operation in some cases. Two experimental approaches are explored.

20. ROIC Developments

Readouts provide the link between a detector array and an imaging system. That link is increasingly becoming digital. Readouts also typically provide bias and preamplification and multiplexing of the detector signals, and are also today capable of providing signal pre-processing on the focal plane—either in analog or digital, or a combination of both. The three papers in this session discuss developments that are increasing the functionality and performance of readout circuits.

A linear-array readout for spectroscopy and machine vision in the SWIR spectral band is described by Goodrich in paper -93. The array format is 1024 pixels long

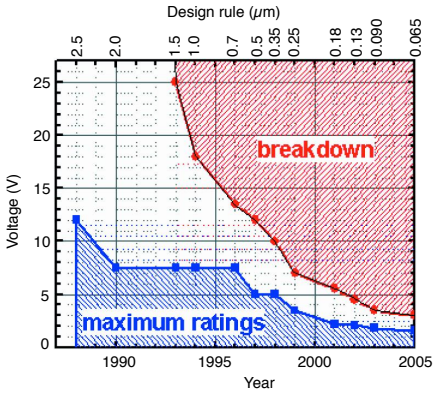

Fig. 37 Shrinking design window of CMOS circuitry used in advanced ROICs as discussed in paper -95.

on a 25 or 50 µm pitch. A CTIA preamplifier provides voltage to current conversion with variable gain in four stages. Amplifier bandwidth is also adjustable.

Paper -94 from LETI reviews their efforts toward the development of nonuniformity or fixed-pattern noise correction using scene-based methods that operate continuously. Analog methods are considered for application to microbolometer detectors—namely adjusting the bias voltage applied to the microbolometer in each pixel.

A description of advanced ROICs for cooled detectors is presented by Sofradir in paper -95. They consider the issues involved in addressing the needs of developing readouts for emerging trends in detectors—dual-band, avalanche photodiodes, larger arrays, and smaller pixel sizes, as well as the increasing use of digital interfaces between the FPA and the imaging system. These issues must be addressed within a shrinking design window for CMOS circuits as illustrated in Fig. 37.

21. Infrared Activities in Japan

A special session on Infrared Activities in Japan was organized by Dr. Masafumi Kimata of Ritsumeikan University.

Paper -96 from NEC presents experiments to detect terahertz radiation from a quantum cascade laser using VO_x microbolometers. At 3.1 THz, the noise equivalent power (NEP) was initially found to be 200 - 300 pW. However, by adding a terahertz absorption layer and by integrating 24 × 24 pixels and 64 frames in a 320 × 240 microbolometer having 23.5 µm pixels, the NEP was reduced to 1 pW. Fig. 38 show the structure of the pixel in cross-section.

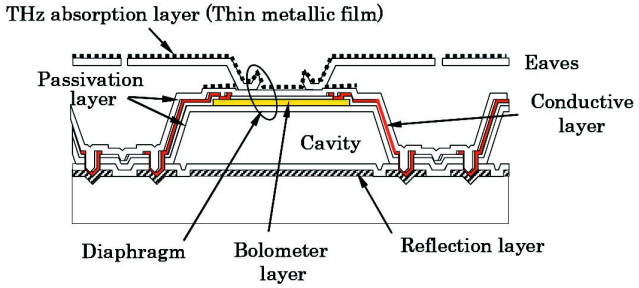

Fig. 38 An uncooled detector pixel from paper -96 modified for the detection of terahertz radiation.

Paper -98 describes the development of an uncooled microbolometer camera for the Japanese Venus orbiter mission PLANET-C. The camera is used to observe the thermal emission from the cloud tops on Venus and to map the cloud top temperature which is as low as 230 K. This is the first application of uncooled microbolometers in Japanese space exploration.

A two-dimensional thermal infrared array sensor called the Infrared Position Sensitive Detector (IRPSD) is reported in paper -99 from Kodenshi and Ritsumeikan University. The IRPSD has two IR thermometers in each pixel: one for the row and one for the column—see Fig. 39. The IR thermometers for each row (or column) are serially connected. The serial connection of the thermometers produces the sum of signals from the pixels in each row and column as shown in Fig. 40. A 10 × 10 IRSPD was fabricated and evaluated. Such a detector has much higher performance than single element IR sensors and is projected to cost much less than large array sensors.

In Paper -100 Nissan Motor describes three types of uncooled thermopile sensors (48 × 32, 120 × 90, and 48 × 48) and their applications in passenger cars. Three types of systems have been developed based on these sensors: a blind spot pedestrian warning system, a rear-view camera system with an IR detection function, and a

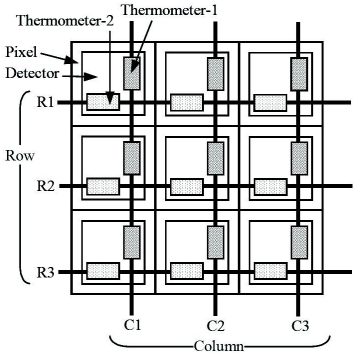

Fig. 39 Block diagram for 3 x 3 IRSPD in Paper-99

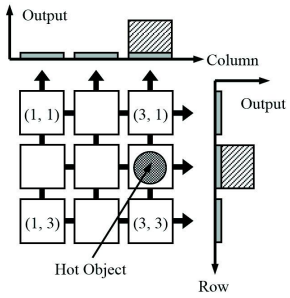

Fig. 40 The method of position detection for a 3 x 3 IRPSD in Paper -99

system that recognizes the driver's hand gestures and enables the driver to control the car's audio and navigation systems without letting go of the steering wheel.

22 and 23. Selected Application Presentations

In papers -101 and -102 the University of Alabama presents a wireless distributed pyroelectric sensor system for identification and tracking of multiple humans in both follow-on and cross-over scenarios. The goal is to replace the more expensive video-based counterparts. The biometric system operates in the 8-10 μm region and uses Fresnel lenses and FOV coding.

A team from the Alabama A&M, Fisk, Boston, and Uzhgorod National Universities, and the Ukranian Institute of Physics discusses, in paper -103, double-channel IR dynamic holographic interferometry. This is an extremely sensitive method for detection of small phase modulation in optical beams. A recent application is the detection of small acoustical vibrations.

NIST, in paper -104, reports on their verification of low measurement uncertainty of newly developed pyroelectric detectors. These detectors are used to extend NIST's reference IR spectral power responsivity scale. It is shown that a relative standard uncertainty of about 0.3% can be achieved in spectral responsivity measurements.

Paper-105 by Sensors Unlimited/Goodrich is concerned with the extension of the InGaAs cut-on wavelength from 0.9 μm to 0.7 μm—see Fig. 41—by removing the bulk InP substrate, leaving only a thin InP contact layer. This extension will improve the overall imaging capability in photon-starved situations and detect illuminators in the 0.8 - 0.9 μm range. New wafer growth and processing methods have been successful. As a result, InGaAs will become a viable alternative or replacement to currently fielded low-light-level systems.

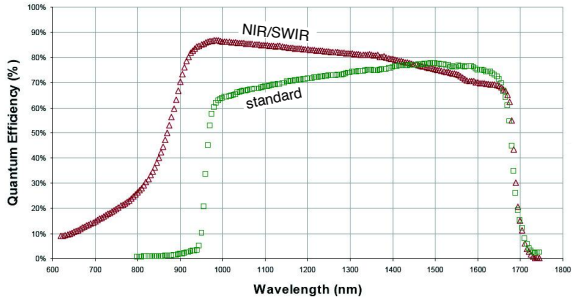

Fig. 41 NIR/SWIR vs. standard SWIR quantum efficiency. From paper -105.

Military IR target acquisition systems require laboratory testing where long target distances are simulated by use of collimators. NIST demonstrates in paper -106 the advantage of using SWIR calibrators for testing MWIR collimators.

The four-channel ColoRad radiometer for measurement of fast transient flashes that was employed for IARD's investigation in paper -55 is described by CI Systems in paper -107. Temporal resolution may be set as low as 5 µsec. The measured temporal behavior of a decoy is given as an example of the radiometer's performance.

24. Selected Technology Presentations

High-speed transparent flexible electronics was the subject of paper -108 from the Univ. of Massachusetts Lowell and Brewer Science. Electronic transistor devices are reported to be formed on a visible-nearIR-transparent film using a solution of carbon nanotubes. Measurements of the transistors gave high values of mobility and frequency response out to ~300 MHz. Inkjet printed circuits are envisioned.

Paper -109 from Virginia Commonwealth Univ. and U.S. Army Research and Development Center reports on rare-earth nanoparticles (10 - 14 nm) for upconversion. The particles are created by laser vaporization. By adjusting the material composition, the photoluminescence properties can be varied widely when pumped with a 980 nm laser diode source.

The development of FPAs from InGaAs, InSb, and HgCdTe is reported in paper -111 from Teledyne Judson. The array format is 320 × 256 with a 30 µm pitch and Indigo readouts are used. The development and characterization of the devices is described, including the temperature dependence of the spectral response.

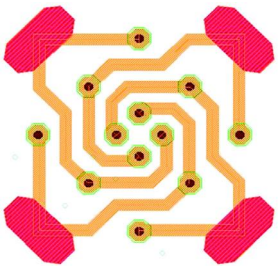

Fig. 42 An example of the layout of four strings of interdigitated subpixel diodes as described in paper -112.

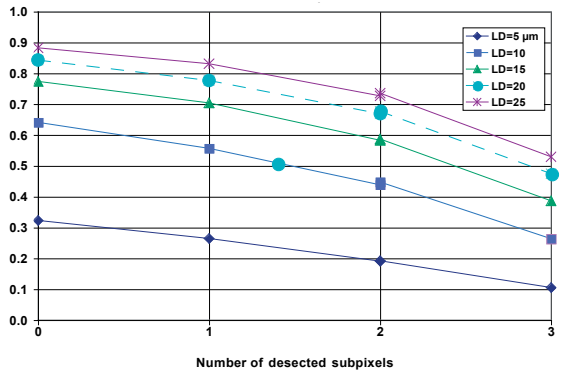

Fig. 43 Calculated collection efficiency as a function of the number of deselected subpixel strings, for five values of the lateral collection length, LD—from paper -112.

In paper -112 DRS addresses the important subject of high operability in VLWIR HgCdTe arrays for meteorological, space defense, and space surveillance applications. Such arrays typically have large pixel sizes and it can be difficult to avoid some bad pixels in such an array, particularly when using VLWIR material. A combination of four small spiral strings of three implanted sub-diodes each are formed for each pixel—see Fig. 42. The subdiodes rely on lateral collection to collect the photo-generated holes. If one, two, or three of the strings are inoperable, the remaining string(s) can still collect a significant percentage of charge, depending upon the lateral diffusion length, as shown in Fig. 43.

Paul R. Norton
Bjørn F. Andresen
Gabor F. Fulop